

# Thermal disorder driven magnetic phases in van der Waals magnet $\text{CrI}_3$

Jaume Meseguer-Sánchez<sup>1</sup>, Dina Abdul Wahab<sup>2</sup>, Hubertus Luetkens<sup>3</sup>, Grigol Taniashvili<sup>4</sup>, Efrén Navarro-Moratalla<sup>1,†</sup>, Zurab Guguchia<sup>3,†</sup>, Elton J. G. Santos<sup>5,†</sup>

<sup>1</sup>*Instituto de Ciencia Molecular, Universitat de València, Calle Catedrático José Beltrán Martínez 2, 46980, Paterna, Spain*

<sup>2</sup>*School of Mathematics and Physics, Queen's University Belfast, BT7 1NN, United Kingdom*

<sup>3</sup>*Laboratory for Muon Spin Spectroscopy, Paul Scherrer Institute, CH-5232 Villigen PSI, Switzerland*

<sup>4</sup>*Department of Physics, Tbilisi State University, Chavchavadze 3, GE-0128 Tbilisi, Georgia*

<sup>5</sup>*Institute for Condensed Matter Physics and Complex Systems, School of Physics and Astronomy, The University of Edinburgh, EH9 3FD, UK*

<sup>†</sup>*Correspondences to: efren.navarro@me.com, zurab.guguchia@psi.ch, esantos@ed.ac.uk*

**Magnetic phase transitions often occur spontaneously at specific critical temperatures and are instrumental to understand the origin of long-range spin order in condensed matter systems. The presence of more than one critical temperature ( $T_c$ ) has been observed in several compounds<sup>1-5</sup> where the coexistence of competing magnetic orders highlights the importance of phase separation driven by different factors such as pressure, temperature and chemical composition. However, it is unknown whether recently discovered two-dimensional (2D) van der Waals (vdW) magnetic materials<sup>6,7</sup> show such intriguing phenomena that can result in**

rich phase diagrams with novel magnetic features to be explored. Here we show the existence of three magnetic phase transitions at different  $T_c$ 's in 2D vdW magnet  $\text{CrI}_3$  revealed by a complementary suite of muon spin relaxation-rotation ( $\mu\text{SR}$ ), superconducting quantum interference device (SQUID) magnetometry, and large-scale micromagnetic simulations including higher-order exchange interactions and dipolar fields<sup>8</sup>. We find that the traditionally identified Curie temperature of bulk  $\text{CrI}_3$  at 61 K<sup>9</sup> does not correspond to the long-range order in the full volume ( $V_M$ ) of the crystal but rather a partial transition with less than  $\sim 25\%$  of  $V_M$  being magnetically spin-ordered. This transition is composed of highly-disordered domains with the easy-axis component of the magnetization ( $S_z$ ) not being fully spin-polarized but disordered by in-plane components ( $S_x, S_y$ ) over the entire layer. As the system cools down, two additional phase transitions at 50 K and 25 K drive the system to 80% and nearly 100% of the magnetically ordered volume, respectively, where the ferromagnetic ground state has a marked  $S_z$  character yet also displaying finite contributions of  $S_x$  and  $S_y$  to the total magnetization. Our results indicate that volume-wise competing electronic phases play an important role in the magnetic properties of  $\text{CrI}_3$  which set a much lower threshold temperature for exploitation in magnetic device-platforms than initially considered.

Competing electronic phases underlie a number of unusual physical phenomena in condensed matter<sup>10–12</sup>. From superconductivity up to ferromagnetism, when the competition is sizeable the conventional outcome is phase separation. Compounds that have shown such behaviour are mostly of complex magnetic structures including cuprates<sup>10</sup>, iron-based superconductors<sup>12</sup>,



ruthenates<sup>11</sup>, topological kagome magnets<sup>3</sup> and manganites<sup>13,14</sup>. A contrasting case is found in the layered transition metal halides<sup>15</sup> where the presence of heavy halide atoms like in CrI<sub>3</sub> stabilises pronounced anisotropy constants resulting in long-range magnetic order in what appears to be a single ferromagnetic transition at a relatively high temperature<sup>6,16</sup>. Nevertheless, recent experiments<sup>17-20</sup> have unveiled the presence of many subtleties in the magnetism of this compound which a single transition fails to capture. Firstly, CrI<sub>3</sub> exhibits both antiferromagnetic and ferromagnetic orders in thin layers driven by hydrostatic pressure<sup>17,18</sup>. These phases occur at the same critical temperature with a spatial separation of a few hundreds of nanometers and consequently there is no prelude of thermally-activated spin ordering. Secondly, multiple anomalies can be observed in the temperature dependence of the magnetic susceptibility below  $T_c$ <sup>9,19,20</sup>. Such anomalies imply that a more complex magnetic ordering involving spins not directly aligned with the easy-axis can emerge. Whether different magnetic phases may exist or competition occurs between them is largely unknown. However, these observations establish a much more intricate scenario than originally pictured for CrI<sub>3</sub> with many hidden features that have important implications in the ordering of the magnetic domains in the system. Here we use high-resolution  $\mu$ SR spectroscopy, complemented by SQUID magnetometry and large scale micromagnetic simulations, to systematically study the thermal evolution of magnetic states in CrI<sub>3</sub>. Such suite is instrumental to identify, characterize and understand distinct macroscopic ground states with any competing magnetic phases.

In a  $\mu$ SR experiment, positive muons implanted into a sample serve as extremely sensitive local microscopic probes to detect small internal magnetic fields and ordered magnetic volume

fractions in the bulk of magnetic systems. See details in *Methods* and Supplementary Sections S1-S2. Zero-field  $\mu$ SR time-spectra are recorded in a powder sample of  $\text{CrI}_3$  below (5 K, 30 K, 54 K and 60 K) and above (65 K and 80 K) the magnetic ordering temperature (Fig. 1a-b). A paramagnetic state is generally characterised by a small Gaussian Kubo-Toyabe depolarization of the muon spin originating from the interaction with randomly oriented nuclear magnetic moments. Conversely, the spectra from the highest measured temperature from 150 K down to 62 K, exhibit a relatively high transverse depolarization rate  $\lambda_T \simeq 4.9(2) \mu\text{s}^{-1}$ . This reflects the occurrence of dense electronic Cr moments and indicates strong interactions between them. In this scenario a novel correlated paramagnetic state may be present in the system at temperatures above the actual Curie temperature. As the crystal is cooled down, in addition to the paramagnetic signal, an oscillating component with a single well defined frequency is observed at  $T \lesssim 62$  K (Fig. 1a-b). Below 50 K, a spontaneous muon spin precession with two well-separated distinct precession frequencies is observed in the  $\mu$ SR spectra and persists down to 5 K. The temperature dependences of the internal fields ( $\mu_0 H_\mu = \omega/\gamma_\mu^{-1}$ ) for the two components are shown in Fig. 2a. The low frequency component shows a monotonous decrease with increasing temperature and disappears at  $T_{C2} \simeq 50$  K. The high frequency component decreases down to 50 K, above which it keeps a constant value within a few Kelvin's range and then decreases again to disappear at  $T_{C1} \simeq 62$  K. Thus, the two oscillatory components have clearly different transition temperatures. This implies the presence of two distinct magnetic transitions in  $\text{CrI}_3$ . We also notice that an upturn on both  $\mu_0 H_{\mu,1}$  and  $\mu_0 H_{\mu,2}$  is seen below  $T_{C3} \simeq 30$  K. Moreover, a strongly damped component appears below  $T_{C3}$  which is seen as some lost of initial asymmetry of the ZF- $\mu$ SR signal. This suggests

the presence of another magnetic transition at this temperature. The temperature dependences of the relative weights of the individual components in the total  $\mu$ SR signal are shown in Fig. 2b. The weight of the high frequency component (component I)  $\omega_1$  gradually increases below  $T_{C1}$  and reaches maximum at  $T_{C2}$ , below which the second frequency appears. The third component raises below  $T_{C3} \simeq 30$  K. The components I and II share the weight of (30 - 70) % in the temperature range between 30 K and 50 K. These results portray the existence of a clear phase diagram in the temperature domain, in excellent agreement with the magnetic singularities observed by SQUID measurements performed in a single crystal of  $\text{CrI}_3$  (see Supplementary Figure S2).

Fig. 2c-d show the temperature dependences of the transverse  $\lambda_T$  and the longitudinal  $\lambda_L$  depolarisation rates, respectively, of components I and II. The  $\lambda_T$  is a measure of the width of the static magnetic field distribution at the muon site, and also reflects dynamical effects (spin fluctuations). The  $\lambda_L$  is determined by dynamic magnetic fluctuations only. For both components,  $\lambda_T$  is higher than  $\lambda_L$  in the whole temperature range, indicating that magnetism is mostly static in origin. However,  $\lambda_{L1}$  has a higher overall value than  $\lambda_{L2}$ , implying that the magnetic order with  $T_{C1} \simeq 62$  K contains more dynamics. The presence of three transitions are clearly substantiated by the anomalies, seen in  $\lambda_T$  and  $\lambda_L$  (Fig. 2c-d). Namely, the  $\lambda_{T,1}$  starts to increase below  $T_{C1}$  and peaks at  $T_{C2}$ , then decreases and tends to saturate. Nevertheless, it increments again below  $T_{C3}$ .  $\lambda_{T,2}$  also exhibits an increase below  $T_{C3}$ . Similarly,  $\lambda_{L,1}$  goes to high values for  $T < T_{C1}$ , saturates at  $T < T_{C2}$  and then enlarges again for  $T < T_{C3}$ , followed by a peak at lower temperature. We note that it is not possible to discriminate in the analysis the contribution of strongly damped components and a high frequency component into  $\lambda_{L1}$  below 30 K and thus the peak in  $\lambda_{L2}$  at low

temperatures could be due to the contribution from component III. Overall, these results point to the complex, unconventional thermal evolution of the magnetic states in  $\text{CrI}_3$ .

The behaviour observed involves a volume-wise interplay between various states, providing an important constraint on theoretical models. One possible interpretation of the data is that below  $T_{C1}$  there is an evolution of the magnetic order in specific volumes of the crystal, which coexists with a correlated paramagnetic state. The second magnetic order thereby occurs within the paramagnetic regions below  $T_{C2}$ . This interpretation is supported by the temperature dependent measurements of the total magnetic fraction  $V_m$  (Fig. 3). The magnetic fraction  $V_m$  does not acquire the full volume below  $T_{C1} \simeq 62$  K. Instead, it gradually increases below  $T_{C1}$  and reaches  $\simeq 80\%$  at  $T_{C2} \simeq 50$  K. An additional increase of  $V_m$  takes place below  $T_{C3} \simeq 25$  K, at which the third strongly damped component appears and reaches nearly  $\simeq 100\%$ . The volume wise evolution of magnetic order across  $T_{C1}$ ,  $T_{C2}$  and  $T_{C3}$  in  $\text{CrI}_3$  strongly suggests the presence of distinct magnetic states in the separate volumes of the sample. In addition, we propose that while the frequency of the second component disappears above 50 K, this component exhibits a precursor correlated state up to the highest temperature investigated 150 K.

To understand the microscopic mechanism of these phase transitions, we undertake macroscale spin dynamics which incorporated atomistic (several Å's) and micromagnetic ( $\mu\text{m}$ -level) underlying details of the magnetic and electronic structure of  $\text{CrI}_3$ . We modelled the atomistic part using strongly correlated density functional theory based on Hubbard- $U$  methods<sup>21</sup> whereas the micromagnetic interactions are described through the Landau-Lifshitz-Gilbert (LLG) equation

techniques<sup>22</sup>. We have also taken into account dipolar fields and higher-order exchange interactions at the level of biquadratic exchange since its sizeable magnitude is important in the magnetic features of 2D magnets<sup>8</sup>. These approaches have been shown to be critical in the description of the spin properties of halide magnets at high-accuracy of critical temperatures, magnetic domains, and topological spin textures<sup>23,24</sup>. See further details in Ref.<sup>8</sup>. We simulated the zero-field cooling processes for a large square flake of bulk  $\text{CrI}_3$  of dimensions  $0.4 \mu\text{m} \times 0.4 \mu\text{m}$  with a thickness above 200 nm thickness to avoid any coexistence of ferro- and anti-ferromagnetic phases in the system<sup>25</sup>. As a descriptor of the spin dynamics of the system we utilize the ratio between the number of spins along the  $z$ -direction or easy-axis  $N(S_z)$ , relative to the total number  $N(S_{\text{total}})$ , that is,  $N(S_z)/N(S_{\text{total}})$ . This allows us to access the number of sites with a specific spin-polarization into the volume of the material which provides information about the disorder caused by thermal fluctuations.

We find that three main phases emerge in  $\text{CrI}_3$  as function of the temperature, which we name them as Disordered-I, Ordered, and Disordered-II (Figure 4). Each phase is labelled according to the degree of deviation relative to the easy-axis of the magnetization  $S_z$  (Fig. 4a). For instance, the Ordered phase is characteristic of magnitudes of  $|S_z|$  with high spin polarization along  $z$ , whereas Disordered-II indicates the opposite. The Disordered-I however sets an intermediate phase between both states with different amount of disorder (Fig. 4b). Surprisingly, the number of spins in the volume of  $\text{CrI}_3$  with  $|S_z| > 0.99$ , corresponding to the full orientation along the easy-axis, is largely a minority ( $N(S_z)/N(S_{\text{total}}) \sim 1.8 - 3.0\%$ ) at the first ( $T_{C1} = 62 \text{ K}$ ) and second ( $T_{C2} = 50 \text{ K}$ ) transitions. Most of the sites have a substantial amount of disorder with spins not completely fol-

lowing the easy-axis of the  $\text{CrI}_3$  but rather stabilising orientations with in-plane orientations ( $S_x$  and  $S_y$ ). Such contributions only become negligible as the temperature drops down below 10 K where a sharp increment of  $N(S_z)/N(S_{\text{total}})$  appears which coincides with the antagonistic response of the Disordered-I phase. Spin sites with larger amount of disorder (e.g. Disordered-II) tend to disappear as the system cools down below 40 K. A spatial visualization of the spin orientations, shown in Fig. 4c for different temperatures confirm this description. Remarkably, it shows that mutually exclusive spatial magnetic regions with distinct projection of the magnetization exist in a wide temperature range, which is in perfect agreement with  $\mu\text{SR}$  results. However, in  $\mu\text{SR}$  the inhomogeneous and mutually exclusive spatial regions exist even at the base- $T$  of 5 K, while the calculations show a sharp increment of the homogeneous  $S_z$ -axis oriented structure below 10 K (Figure 4b). The reason for this discrepancy could be that: (i) there is not a one-to-one correspondence in the temperature values between experiment and theory. (ii) In reality, much lower temperatures than 5 K are most likely required to get homogeneous magnetic states. It is worth mentioning that even when the system reached 0 K, where thermal fluctuations are inexistent, the spins still evolve in time as an effect due to high magnetic anisotropy and meta-stability of the magnetic domains in  $\text{CrI}_3$ <sup>23</sup> (Fig. 4c). Our results suggest that the magnetic structure of bulk  $\text{CrI}_3$  is markedly composed by thermal disorder with no apparent formation of anti-ferromagnetic phases as observed in few layers<sup>6,17,18,25</sup>.

## **Supplementary Materials**

Materials and Methods.

Supplementary sections S1 to S5, and Figures S1-S2.

### **0.0.1 Data Availability**

The data that support the findings of this study are available within the paper and its Supplementary Information.

### **0.0.2 Competing interests**

The Authors declare no conflict of interests.

### **0.0.3 Acknowledgments**

$\mu$ SR experiments were performed at the  $\pi$ M3 beam line (low background GPS instrument) of the Swiss Muon Source (SmuS) of the Paul Scherrer Institute, Villigen, Switzerland, under proposal ID: 20190297 with EJGS as the PI. GT thank Prof. Alexander Shengelaya and the Georgian National Science Foundation (grant PHDF-19-060) for funding support to participate in  $\mu$ SR experiments led by ZG and EJGS. EJGS acknowledges computational resources through the UK Materials and Molecular Modelling Hub for access to THOMAS supercluster, which is partially

funded by EPSRC (EP/P020194/1); CIRRUS Tier-2 HPC Service (ec131 Cirrus Project) at EPCC (<http://www.cirrus.ac.uk>) funded by the University of Edinburgh and EPSRC (EP/P020267/1); ARCHER UK National Supercomputing Service (<http://www.archer.ac.uk>) via Project d429. EJGS acknowledges the EPSRC Early Career Fellowship (EP/T021578/1) and the University of Edinburgh for funding support. ENM acknowledges the European Research Council (ERC) under the Horizon 2020 research and innovation programme (ERC StG, grant agreement No. 803092).

## References and Notes

1. Luetkens, H. *et al.* Microscopic evidence of spin state order and spin state phase separation in layered cobaltites  $rbaco_2o_{5.5}$  with  $r = y, tb, dy, \text{ and } ho$ . *Phys. Rev. Lett.* **101**, 017601 (2008). URL <https://link.aps.org/doi/10.1103/PhysRevLett.101.017601>.
2. Hiraishi, M. *et al.* Bipartite magnetic parent phases in the iron oxypnictide superconductor. *Nature Physics* **10**, 300–303 (2014). URL <https://doi.org/10.1038/nphys2906>.
3. Guguchia, Z. *et al.* Tunable anomalous hall conductivity through volume-wise magnetic competition in a topological kagome magnet. *Nature Communications* **11**, 559 (2020). URL <https://doi.org/10.1038/s41467-020-14325-w>.
4. Guguchia, Z. *et al.* Magnetism in semiconducting molybdenum dichalcogenides. *Science Advances* **4** (2018). URL <https://advances.sciencemag.org/content/4/12/eaat3672>.  
<https://advances.sciencemag.org/content/4/12/eaat3672.full.pdf>.



5. Niedermayer, C. *et al.* Common phase diagram for antiferromagnetism in  $\text{La}_{2-x}\text{Sr}_x\text{CuO}_4$  and  $\text{Y}_{1-x}\text{Ca}_x\text{Ba}_2\text{Cu}_3\text{O}_6$  as seen by muon spin rotation. *Phys. Rev. Lett.* **80**, 3843–3846 (1998). URL <https://link.aps.org/doi/10.1103/PhysRevLett.80.3843>.
6. Huang, B. *et al.* Layer-dependent ferromagnetism in a van der waals crystal down to the monolayer limit. *Nature* **546**, 270–273 (2017).
7. Gong, C. *et al.* Discovery of intrinsic ferromagnetism in two-dimensional van der waals crystals. *Nature* **546**, 265–269 (2017). URL <http://dx.doi.org/10.1038/nature22060>. Letter.
8. Kartsev, A., Augustin, M., Evans, R. F. L., Novoselov, K. S. & Santos, E. J. G. Biquadratic exchange interactions in two-dimensional magnets. *npj Computational Materials* **6**, 150 (2020). URL <https://doi.org/10.1038/s41524-020-00416-1>.
9. McGuire, M. a., Dixit, H., Cooper, V. R. & Sales, B. C. Coupling of crystal structure and magnetism in the layered, ferromagnetic insulator  $\text{CrI}_3$ . *Chem. Mater.* **27**, 612–620 (2015).
10. Mohottala, H. E. *et al.* Phase separation in superoxygenated  $\text{La}_{2-x}\text{Sr}_x\text{CuO}_{4+y}$ . *Nature Materials* **5**, 377–382 (2006). URL <https://doi.org/10.1038/nmat1633>.
11. Uemura, Y. J. *et al.* Phase separation and suppression of critical dynamics at quantum phase transitions of  $\text{mnsi}$  and  $(\text{sr}_{1-x}\text{ca}_x)\text{ruo}_3$ . *Nature Physics* **3**, 29–35 (2007). URL <https://doi.org/10.1038/nphys488>.

12. de la Cruz, C. *et al.* Magnetic order close to superconductivity in the iron-based layered  $\text{LaO}_{1-x}\text{F}_x$  systems. *Nature* **453**, 899–902 (2008). URL <https://doi.org/10.1038/nature07057>.
13. Milward, G. C., Calderón, M. J. & Littlewood, P. B. Electronically soft phases in manganites. *Nature* **433**, 607–610 (2005). URL <https://doi.org/10.1038/nature03300>.
14. Uehara, M., Mori, S., Chen, C. H. & Cheong, S. W. Percolative phase separation underlies colossal magnetoresistance in mixed-valent manganites. *Nature* **399**, 560–563 (1999). URL <https://doi.org/10.1038/21142>.
15. de Jongh, L. *Magnetic Properties of Layered Transition Metal Compounds* (Springer, 2012).
16. Dillon, J. F. & Olson, C. E. Magnetization, resonance, and optical properties of the ferromagnet  $\text{CrI}_3$ . *J. Appl. Phys.* **36**, 1259–1260 (1965).
17. Song, T. *et al.* Switching 2d magnetic states via pressure tuning of layer stacking. *Nature Materials* **18**, 1298–1302 (2019). URL <https://doi.org/10.1038/s41563-019-0505-2>.
18. Li, T. *et al.* Pressure-controlled interlayer magnetism in atomically thin  $\text{CrI}_3$ . *Nature Materials* **18**, 1303–1308 (2019). URL <https://doi.org/10.1038/s41563-019-0506-1>.
19. Liu, Y. & Petrovic, C. Anisotropic magnetocaloric effect in single crystals of  $\text{CrI}_3$ . *Phys. Rev. B Condens. Matter* **97**, 174418 (2018).
20. Wang, Z. *et al.* Very large tunneling magnetoresistance in layered magnetic semiconductor  $\text{CrI}_3$ . *Nat. Commun.* **9**, 2516 (2018).

21. Dudarev, S. L., Botton, G. A., Savrasov, S. Y., Humphreys, C. J. & Sutton, A. P. Electron-energy-loss spectra and the structural stability of nickel oxide: An lsd+u study. *Phys. Rev. B* **57**, 1505–1509 (1998). URL <https://link.aps.org/doi/10.1103/PhysRevB.57.1505>.
22. Nakatani, Y., Uesaka, Y. & Hayashi, N. Direct solution of the landau-lifshitz-gilbert equation for micromagnetics. *Japanese Journal of Applied Physics* **28**, 2485–2507 (1989). URL <https://doi.org/10.1143/JJAP.28.2485>.
23. Wahab, D. A. *et al.* Quantum rescaling, metastability and hybrid domain-walls in two-dimensional  $\text{CrI}_3$  magnets. *arXiv*: (2020).
24. Augustin, M., Jenkins, S., Evans, R. F. L., Novoselov, K. S. & Santos, E. J. G. Properties and dynamics of meron topological spin textures in the two-dimensional magnet  $\text{CrI}_3$ . *arXiv*: (2020).
25. Niu, B. *et al.* Coexistence of magnetic orders in two-dimensional magnet  $\text{CrI}_3$ . *Nano Letters* **20**, 553–558 (2020). URL <https://doi.org/10.1021/acs.nanolett.9b04282>.

## Figure captions

Figure 1:  **$\mu$ SR spectroscopy applied to  $\text{CrI}_3$ .** **a-b**, Zero-field  $\mu$ SR spectra, recorded at various temperatures for the polycrystalline sample of  $\text{CrI}_3$ , shown in the low and extended time interval. The solid lines are the fit of the data using the methods of Supplementary Sections S3-S4. Error bars are the standard error of the mean in about  $10^6$  events. The error of each bin count is given by the standard deviation of  $n$ . The errors of each bin in the  $\mu$ SR asymmetry are then calculated by statistical error propagation.

Figure 2: **Temperature dependent  $\mu$ SR parameters.** **a**, The temperature dependence of the internal magnetic fields for the observed two components in  $\text{CrI}_3$ . **b**, The temperature dependence of the relative weights of the three components in the total signal for  $\text{CrI}_3$ , determined from zero-field  $\mu$ SR experiments. **c-d**, The temperature dependence of transverse depolarization rates  $\lambda_{T1}$ ,  $\lambda_{T2}$  and the longitudinal depolarization rates  $\lambda_{L1}$ ,  $\lambda_{L2}$  for two components. The error bars represent the standard deviation of the fit parameters.

Figure 3: **Thermal evolution of various magnetic phases in  $\text{CrI}_3$ .** **a**, The temperature dependence of the total magnetic volume fraction  $V_M$ , determined from precise weak transverse field (weak-TF)  $\mu$ SR measurements. In this weak-TF experiment, a small magnetic field of 30 G is applied nearly perpendicular to the muon spin polarisation. The different components seen in Fig. 2 are highlighted in each region of the temperature range with the paramagnetic phase above the Curie temperature. The error bars represent the standard deviation of the fit parameters.

Figure 4: **Micromagnetic analysis of the spin dynamics in CrI<sub>3</sub>.** **a**, Diagram of the different magnitudes of  $|S_z|$  relative to the unit sphere in the range of  $|S_z| = 1$  (full polarized along  $z$ ) and  $|S_z| = 0$  (only in-plane  $xy$ -projections). The orientations of the spins are assigned randomly following the Monte Carlo moves. The plot only shows a schematic of possible projections over the sphere with others (not shown) with the same  $|S_z|$  equally probable. **b**, Magnetic fraction (in %) of the out-of-plane spins ( $N(S_z)/N(S_{\text{total}})$ ) as a function of the temperature. The calculation of  $N(S_z)$  and  $N(S_{\text{total}})$  take into account the volumetric amount of spins over the entire system for  $S_z$  and  $S_{\text{total}}$ , respectively. Three main phases were identified in bulk CrI<sub>3</sub> which are named: Disordered-I (faint black), with values of  $N(S_z)/N(S_{\text{total}})$  between the curves of  $0.01 < |S_z| < 0.99$  and  $0.20 < |S_z| < 0.80$ ; Ordered (faint red), within  $|S_z| > 0.80$  and  $|S_z| > 0.99$ ; and, Disordered-II (faint blue), within  $|S_z| < 0.01$  and  $|S_z| < 0.20$ . The solid curves showed in each phase provide a sample of a specific variation of  $N(S_z)/N(S_{\text{total}})$  for a given range of  $|S_z|$ . The vertical dashed line sets the time of 2 ns required to achieve 0 K in the spin dynamics. The magnitudes of  $N(S_z)/N(S_{\text{total}})$  showed after 0 K demonstrated that even when the thermal fluctuations are zero, the system is still evolving to stabilize its ground state. The critical temperatures ( $T_{C1,C2,C3}$ ) are also highlighted. **c**, Snapshots of the dynamical spin configurations of bulk CrI<sub>3</sub> during field cooling from 80 K down to 0 K. Magnetisation is projected along of in-plane components ( $S_x$ ,  $S_y$ ) and  $S_z$  at different temperatures: 68 K, 60 K, 50 K, 20 K and 0 K. Each column and row corresponds to a specific projection of the magnetization at a given temperature provided at the far left. The colour scale shows the variation of the three magnetization components ( $S_x$ ,  $S_y$ ,  $S_z$ ) throughout the system.

## Figures

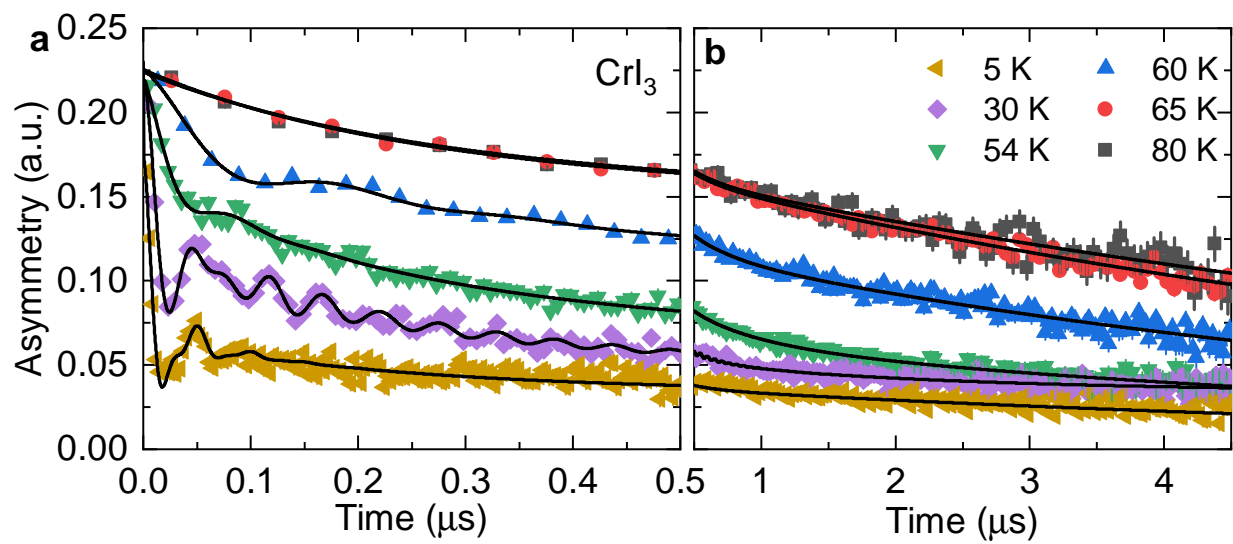


Figure 1

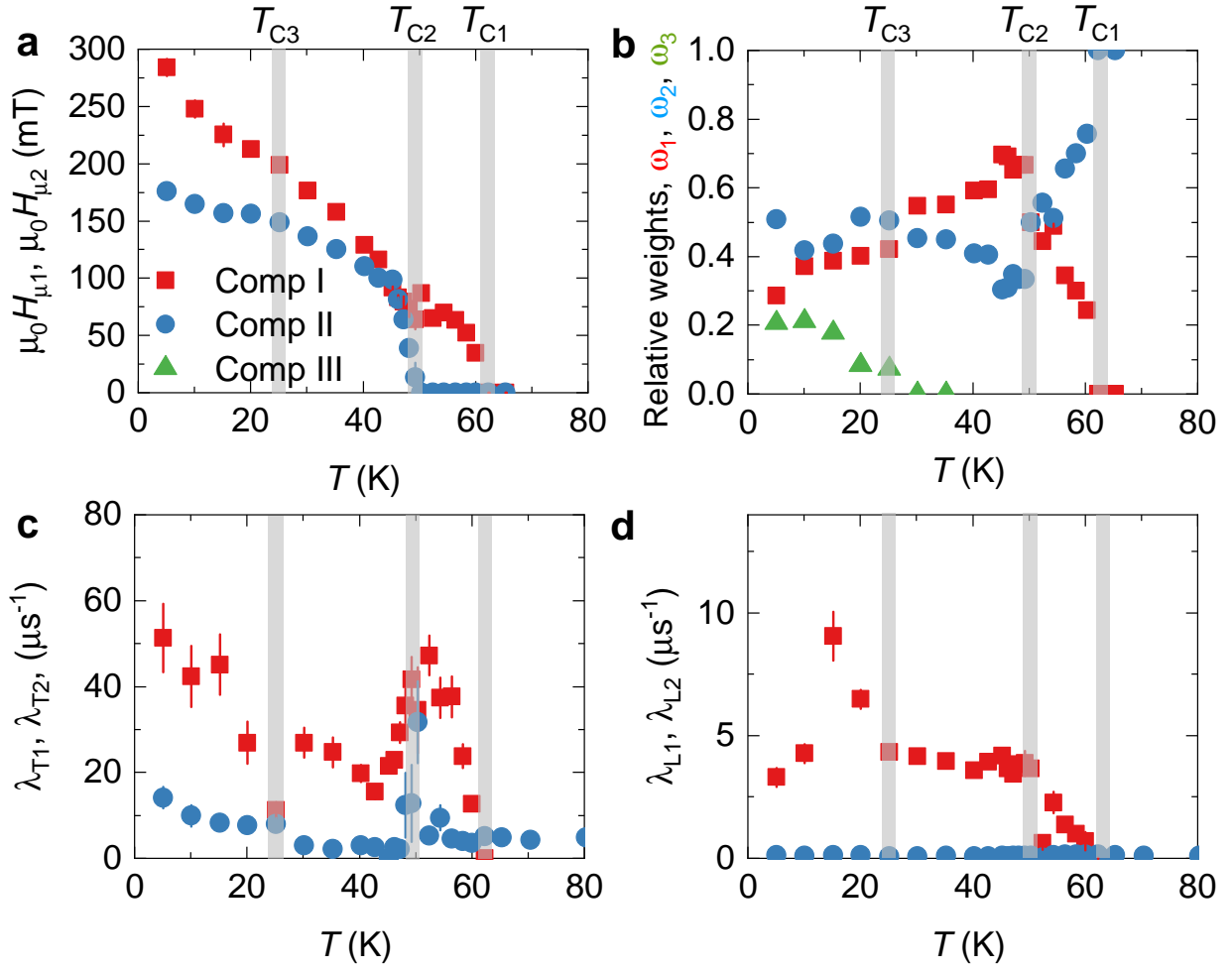


Figure 2

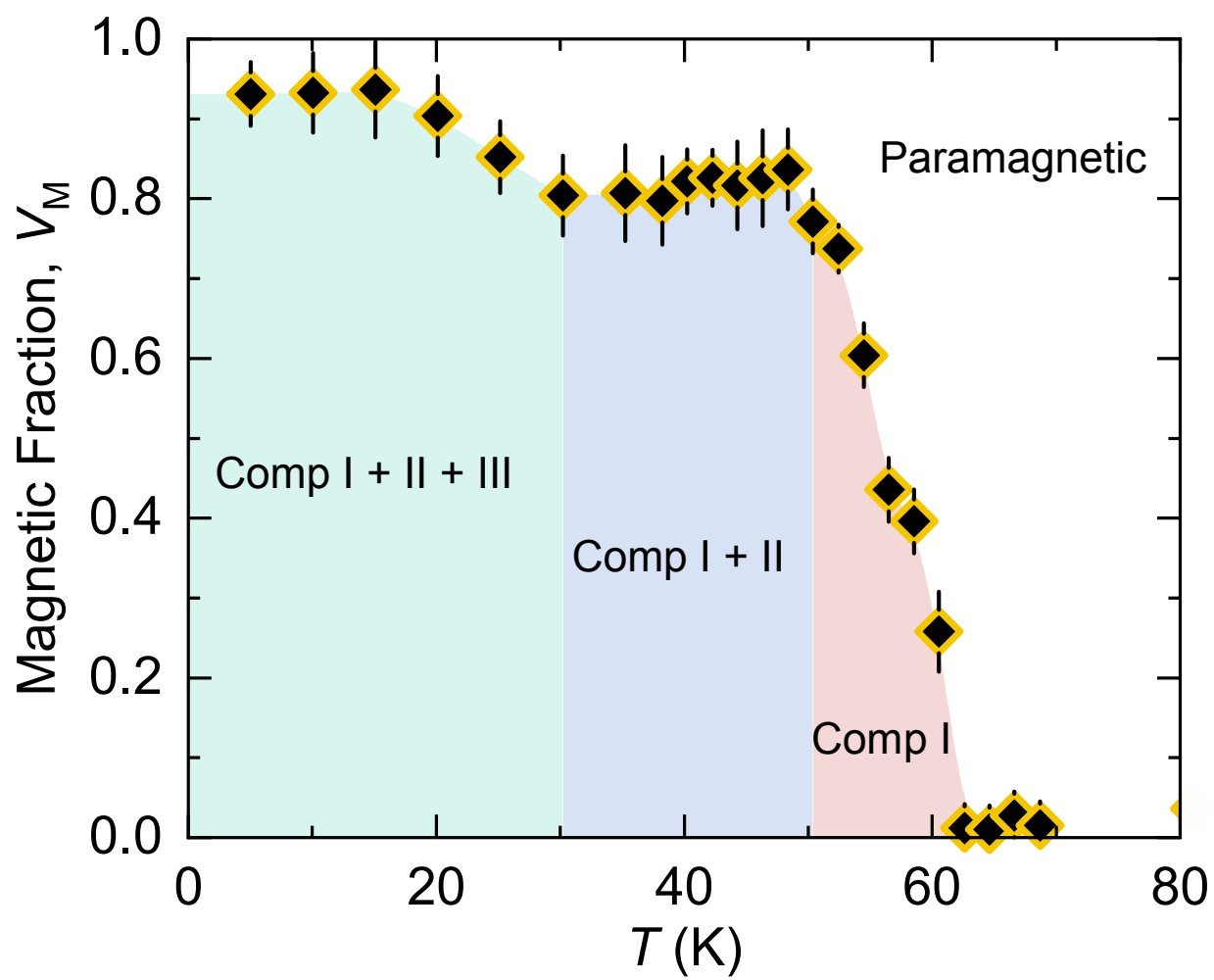


Figure 3



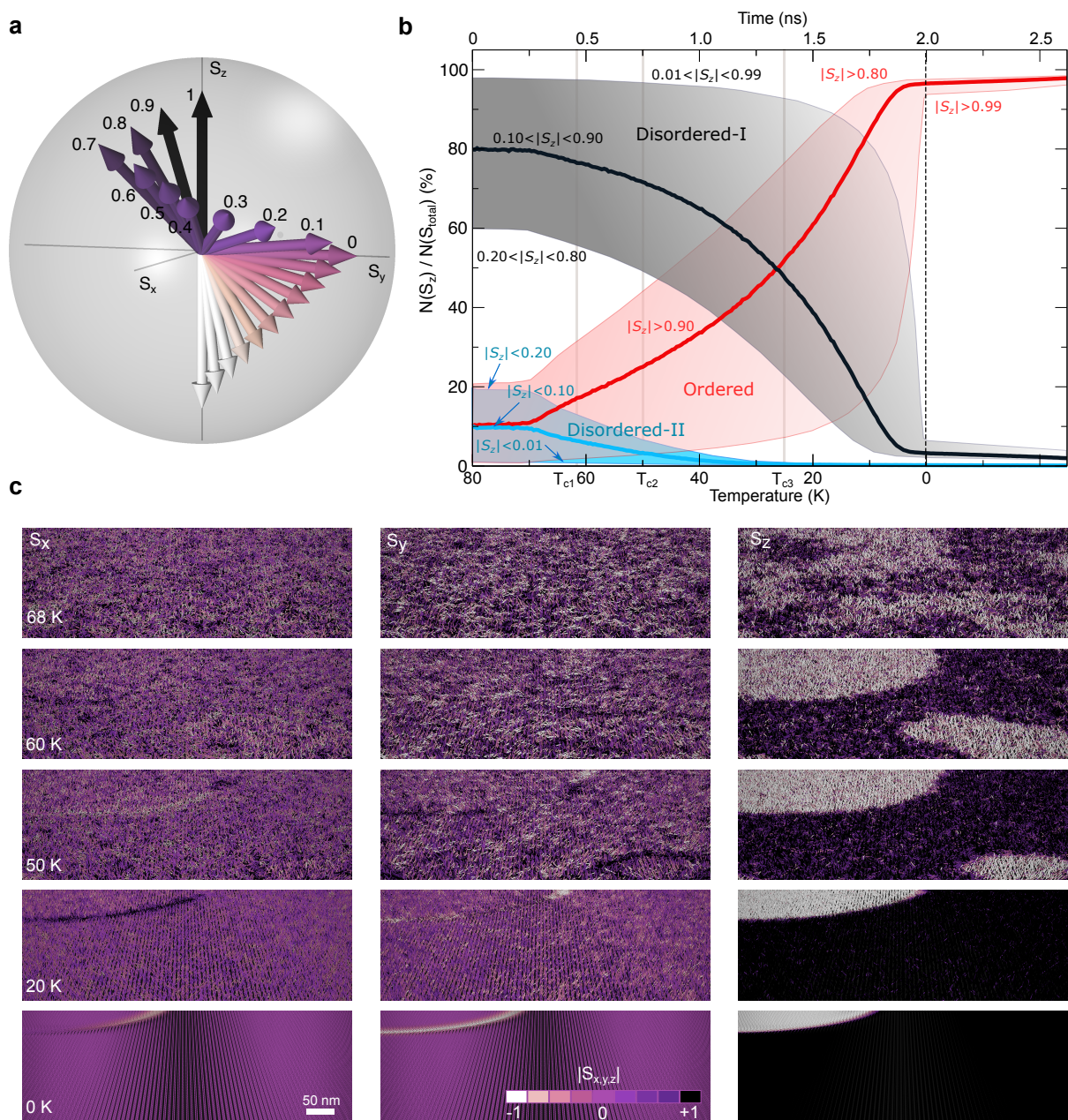


Figure 4